

The AGILE monitoring of Cygnus X-3: transient gamma-ray emission and spectral constraints

G. Piano^{1,2}, M. Tavani^{1,2,3,8}, V. Vittorini¹, A. Trois⁹, A. Giuliani⁴, A. Bulgarelli⁵, Y. Evangelista¹, P. Coppi¹⁵, E. Del Monte¹, S. Sabatini^{1,2,8}, E. Striani^{3,8}, I. Donnarumma¹, D. Hannikainen^{16,17}, K. I. I. Koljonen¹⁶, M. McCollough¹⁸, G. Pooley¹⁹, S. Trushkin²⁰, R. Zanin²¹, G. Barbiellini⁶, M. Cardillo^{1,3}, P. W. Cattaneo⁷, A. W. Chen⁴, S. Colafrancesco^{12,13}, M. Feroci¹, F. Fuschino⁵, M. Giusti^{1,2}, F. Longo⁶, A. Morselli⁸, A. Pellizzoni⁹, C. Pittori^{11,12}, G. Pucella¹⁰, M. Rapisarda¹⁰, A. Rappoldi⁷, P. Soffitta¹, M. Trifoglio⁵, S. Vercellone¹⁴, and F. Verrecchia^{11,12}

(Affiliations can be found after the references)

Preprint online version: March 24, 2022

ABSTRACT

We present the AGILE-GRID monitoring of Cygnus X-3, during the period between November 2007 and July 2009. We report here the whole AGILE-GRID monitoring of Cygnus X-3 in the AGILE “pointing” mode data-taking, in order to confirm that the γ -ray activity occurs in coincidence with the same repetitive pattern of multiwavelength emission and to analyze in depth the overall γ -ray spectrum by assuming both leptonic and hadronic scenarios. Seven intense γ -ray events were detected in this period, with a typical event lasting 1 or 2 days. Such a duration is longer than the likely cooling times of the γ -ray emitting particles, implying we are seeing continuous acceleration rather than the result of an impulsive event such as the ejection of a single plasmoid which then cools as it propagates outwards. Cross-correlating the AGILE-GRID light curve with X-ray and radio monitoring data, we find that the main events of γ -ray activity have been detected while the system was in soft spectral X-ray states ($RXTE/ASM$ count rate ≥ 3 counts s^{-1}), coincident with local and often sharp minima of the hard X-ray flux ($Swift/BAT$ count rate ≤ 0.02 counts $cm^{-2} s^{-1}$), a few days before intense radio outbursts. This temporal repetitive coincidence between γ -ray transient emission and spectral state changes of the source turns out to be the *spectral signature* of the γ -ray activity from this microquasar. The γ -ray events thus may reflect a sharp transition in the structure of the accretion disk and its corona, which leads to a rebirth of the microquasar jet and subsequent enhanced radio activity. The γ -ray differential spectrum of Cygnus X-3 (100 MeV – 3 GeV), obtained by averaging the data collected by the AGILE-GRID during the γ -ray events, is consistent with a power law of photon index $\alpha = 2.0 \pm 0.2$. Finally, we examine leptonic and hadronic emission models for the γ -ray events and find that both scenarios may work. In the leptonic model – based on IC scatterings of mildly relativistic electrons on soft photons from the Wolf-Rayet companion star and from the accretion disk – the emitting particles may also contribute to the overall hard X-ray spectrum, possibly explaining the hard non-thermal power-law tail sometimes seen during special soft X-ray states in Cygnus X-3.

Key words. stars: individual: Cygnus X-3 – gamma rays: general – X-rays: binaries – radio continuum: general – radiation mechanisms: non-thermal – stars: winds, outflows

1. Introduction

Cygnus X-3 is the brightest radio source among microquasars and it was discovered, as an X-ray source, in 1966 (Giacconi et al., 1967). It is a high mass X-ray binary: the companion star is a Wolf-Rayet (WR) star (van Kerkwijk et al., 1992) with a strong stellar helium wind (Szostek & Zdziarski, 2008). The system is located at a distance of about 7-10 kpc (Bonnet-Bidaud & Chardin, 1988; Ling et al., 2009). The orbital period is 4.8 hours, inferred from infrared (Becklin et al., 1973), X-ray (Parsignault et al., 1972) and γ -ray (Abdo et al., 2009) observations. Due to the very tight orbit (orbital distance $d \approx 3 \times 10^{11}$ cm), the compact object is totally enshrouded in the wind of the companion star¹. The nature of the compact object is still uncertain² (Vilhu et al., 2009), even if a black hole scenario is favored (Szostek & Zdziarski, 2008; Szostek et al., 2008). In

the radio band the system shows strong flares (“major radio flares”) reaching up to few tens of Jy. Radio observations at milliarcsec scales confirm emissions (at cm wavelengths) from both a core and a one-sided relativistic jet ($v \sim 0.81c$), with an inclination to the line-of-sight of $\lesssim 14^\circ$ (Mioduszewski et al., 2001). The radiation from the jet dominates the radio emission from the core during (and soon after) the major flares (Tudose et al., 2010).

Cygnus X-3 exhibits a clear and repetitive pattern of (anti)correlations between radio and X-ray emission, and an overall anticorrelation between soft and hard X-ray fluxes (McCollough et al., 1999; Szostek et al., 2008). The most important pattern of correlations found by Szostek et al. (2008) is related to the connection between radio (8.3 GHz band, GBI) and soft X-ray emissions (3-5 keV band, $RXTE/ASM$). When the soft X-ray flux is above the transition level (3 counts/s), the source can be found in different states, depending on the level of the radio flux density. In particular, the *quenched state* is characterized by a radio flux density ≤ 30 mJy and it is followed by a *major-flaring state* with values of the radio flux density ≥ 1 Jy. It is very important to emphasize that all major radio flares have been observed after a quenched state, and in almost all cases the quenched state is followed by a major flare. After a

¹ The observational evidence of this strong wind can be found in the prominent attenuation of the Cygnus X-3 power density spectrum (PDS) for frequencies above 0.1 Hz (Axelsson et al., 2009; Koljonen et al., 2011).

² Published results suggest either a neutron star of $1.4 M_\odot$ (Stark & Saia, 2003) or a black hole with a mass $\leq 10 M_\odot$ (Hanson et al., 2000; Shrader et al., 2010).

major flare a “*hysteresis*” in the radio/soft-X-ray plane is found: the decline of the radio flux density never occurs through a quenched state.

Firm detections of high-energy γ -rays (HE γ -rays: >100 MeV) from Cygnus X-3³ have been published at the end of 2009: the AGILE Team found evidence of strong γ -ray transient emission above 100 MeV in coincidence with special X-ray/radio spectral states (Tavani et al., 2009a), and the Fermi-LAT collaboration announced the detection of the γ -ray orbital modulation (Abdo et al., 2009). The peak γ -ray isotropic luminosity detected above 100 MeV is $L_\gamma \sim 10^{36}$ erg s⁻¹ (for a distance of 7-10 kpc). The γ -ray emission is most likely associated with relativistic jet (Tavani et al., 2009a; Abdo et al., 2009; Dubus et al., 2010; Cerutti et al., 2011; Zdziarski et al., 2012), but the radiative process (leptonic or hadronic) is not certain.

A possible leptonic scenario for γ -ray emission in Cygnus X-3 was proposed by Dubus et al., 2010: stellar UV photons are Compton upscattered to HE by relativistic electrons accelerated in the jet. The particle acceleration could take place in a shock where the jet interacts with the dense stellar wind of the WR star. The jet – with moderate bulk relativistic speed – is oriented not too far from the line-of-sight. According to this model, Cygnus X-3 is a *microblazar*, with a jet pointing towards the Earth.

The γ -ray modulation – coherent with the orbital period – suggests that the emitting region is located between $\sim 10^{10}$ cm and $\sim 3 \times 10^{12}$ cm (10d) to the compact object (Dubus et al., 2010; Cerutti et al., 2011). The lack of modulation at radio wavelengths and the delay (~ 5 days, Abdo et al., 2009) between the onset of γ -ray activity and the radio flare suggest different emission regions linked by the collimated jet. The γ -ray emission – related to inverse Compton (IC) scatterings – most likely occurs close to the compact object, while the radio emission – assumed to be synchrotron in origin – occurs farther out in the jet, at an angular distance from the core of few tens of milli-arcsec (e.g., Tudose et al., 2007, 2010), corresponding to $\sim 10^{15}$ – 10^{16} cm. The γ -ray modulation is due to the anisotropic efficiency of the IC scattering (Aharonian & Atoyan, 1981). Thus, the γ -ray maximum occurs at the superior conjunction (compact object behind the WR star), when relativistic electrons of the jet, moving towards the Earth, have head-on collision with UV stellar photons. This orbital phase corresponds to the minimum of the X-ray modulation, due to the maximum absorption/scattering by the companion’s wind (Abdo et al., 2009; Dubus et al., 2010; Zdziarski et al., 2012).

A hadronic scenario accounting for γ -ray emission in the context of microquasars was discussed by e.g. Romero et al. (2003, 2005). The model is based on the interaction of a mildly relativistic jet with the dense wind of the companion star. γ -ray emission is due to the decay of neutral pions (π^0) produced by pp collisions.

³ γ -ray detections of Cygnus X-3 were reported in the 1970s and in the 1980s at TeV (Vladimirsky et al., 1973; Danaher et al., 1981; Lamb et al., 1982) and PeV energies (Samorski & Stamm, 1983; Bhat et al., 1986). However, subsequent observations by more sensitive ground-based telescopes did not confirm TeV and PeV emission from the source (O’Flaherty et al., 1992). Furthermore, the *COS-B* satellite could not find any clear emission from Cygnus X-3 at MeV-GeV energies (Hermesen et al., 1987), and both *CGRO*/EGRET observations of the Cygnus region (1991-1994) and the first-year analysis of AGILE observations could not demonstrate a solid association with the microquasar, although confirming a γ -ray detection above 100 MeV in a region including Cygnus X-3 (Mori et al., 1997; Pittori et al., 2009).

Furthermore, TeV emission from relativistic jet in microquasars has been predicted by several models (e.g., see Atoyan & Aharonian, 1999). A search for very-high-energy (VHE) γ -rays from microquasar GRS 1915+105 with the HESS Cherenkov telescope has been carried out, but no significant detection was found in the direction of the source (H.E.S.S. Collaboration et al., 2009). On the other hand, hints of VHE γ -rays were found in Cygnus X-1 (Albert et al., 2007). MAGIC observed Cygnus X-3 several times between March 2006 and August 2009, during both hard and soft states⁴, but no evidence of clear VHE γ -ray emission from the microquasar was found: an overall 2σ upper limit to the integral flux has been set to 2.2×10^{-12} photons cm⁻² s⁻¹ for energies above 250 GeV (Aleksić et al., 2010).

Here we present a comprehensive and homogeneous analysis of Cygnus X-3 which takes into account γ -ray events found in the data between 2007-November-02 and 2009-July-29, during the AGILE “pointing” mode data-taking. We analyzed a dataset previously published by Tavani et al. (2009a) and Bulgarelli et al. (2012a). We report here the whole AGILE-GRID monitoring of Cygnus X-3 during the “pointing” mode, in order to confirm that the γ -ray activity occurs in coincidence with the same repetitive pattern of multiwavelength emission and to analyze in depth the overall γ -ray spectrum by assuming both leptonic and hadronic scenarios.

2. Observations

The AGILE scientific instrument (Tavani et al., 2009b) is very compact and is characterized by two co-aligned imaging detectors operating in the energy ranges 30 MeV–30 GeV (GRID: Barbiellini et al., 2002; Prest et al., 2003) and 18–60 keV (Super-AGILE: Feroci et al., 2007), as well as by an anticoincidence system (Perotti et al., 2006) and a calorimeter (Labanti et al., 2006). AGILE’s performance is characterized by large fields of view (2.5 and 1 sr for the γ -ray and hard X-ray bands, respectively) and optimal angular resolution (PSF = 3.0° at 100 MeV and PSF = 1.5° at 400 MeV, see Cattaneo et al., 2011).

AGILE operated in “pointing” mode with fixed attitude until mid-October, 2009; in November, 2009 AGILE entered in “scanning mode”, characterized by a controlled rotation of the pointing axis.

During the “pointing” mode data-taking (~ 2.5 years) the AGILE satellite performed ~ 100 pointings with variable exposure times (typically 3–30 days), drifting about 1 degree per day with respect to the initial boresight direction to match solar panel illumination constraints⁵. In this configuration the AGILE-GRID was characterized by enhanced performances in the monitoring capability of a given source, especially in the energy band 100–400 MeV (see Bulgarelli et al., 2012a for details). Due to the different pointing strategies between the AGILE and Fermi satellites, the high on-source cumulative exposure (between 100 and 400 MeV) of the AGILE-GRID may be fundamental in the observation of this particular source.

In this paper we report an analysis based on the AGILE-GRID data collected between 2007-November-02 and 2009-July-29 (the same dataset reported by Chen, Piano et al., 2011).

⁴ The MAGIC telescope also pointed at Cygnus X-3 after two γ -ray alerts from the AGILE-GRID team (the first one after the γ -ray event of 16-17 April 2008, the second after the event of 13-14 July 2009, see Appendix A). In both cases they found a 2σ upper limit, for energies above 250 GeV, of $\sim 10^{-11}$ photons cm⁻² s⁻¹ (Aleksić et al., 2010).

⁵ A detailed schedule of the AGILE observations – with the pointing starting coordinates and observation’s starting and ending times – is available online at http://agile.asdc.asi.it/current_pointing.html

During this period AGILE repeatedly pointed at the Cygnus region for a total of ~ 275 days, corresponding to a net exposure time of ~ 11 Ms. The detailed analysis of the dataset is presented in Appendix A. In this paper we report 7 γ -ray main events.

3. The gamma-ray activity in a multiwavelength context

3.1. General characteristics of the gamma-ray events

Figure 1 shows the comprehensive multiwavelength light curve of Cygnus X-3, in order to analyze the pattern of emission. The γ -ray activity detected by the AGILE-GRID is presented along with hard X-ray fluxes from *Swift*/BAT⁶ (15-50 keV), soft X-ray fluxes from *RXTE*/ASM⁷ (3-5 keV) and radio flux density (when available) from AMI-LA⁸ (15 GHz) and RATAN-600⁹ (2.15, 4.8, 11.2 GHz) radio telescopes.

The aim of the cross-correlation between the AGILE-GRID light curve and the multiwavelength emission pattern is to discuss the γ -ray trigger criteria and to compare them with the ones previously published by Tavani et al., 2009a; Bulgarelli et al., 2012a; Corbel et al., 2012.

Observing the light curve in Figure 1, as well as the detailed zooms in Figure 2, we notice that:

- there is a *strong anticorrelation* between hard X-ray and γ -ray emission. Every local minimum of the hard X-ray light curve is associated with γ -ray emission detected by the AGILE-GRID (see also the weak γ -ray event detected on 2008-June-21, MJD = 54638.58, in the plot of Figure 1: $\sqrt{TS} = 2.77$, photon flux = $(131 \pm 61) \times 10^{-8}$ photons cm⁻² s⁻¹). Vice versa, every time the AGILE-GRID detects γ -ray activity the system exhibits a deep local minimum of the hard X-ray light curve (*Swift*/BAT count rate $\lesssim 0.02$ counts cm⁻² s⁻¹).
- Every time we detect γ -ray activity, Cygnus X-3 is in a soft spectral state (*RXTE*/ASM count rate $\gtrsim 3$ counts s⁻¹, i.e., the transitional level defined by Szostek et al., 2008).
- Every time we detect γ -ray episodes (Table A.1 and red points in the AGILE-GRID light curve in Figure 1) the system is moving to a major radio flare (radio flux density $\gtrsim 1$ Jy) or to a quenched state preceding a major radio flare.

In Table 1 we report a brief synthesis of the multi-frequency pattern of emission of each main γ -ray event ($\sqrt{TS} \gtrsim 3$) detected by the AGILE-GRID. The average value of the delay between the γ -ray event and the subsequent radio flare is $\Delta T_2 \approx 4$ days, consistent with the value (5 ± 7 days) found by Abdo et al. (2009). If we refer to the third column in Table 1, we can see that the transient γ -ray emission occurs when the system is moving into a quenched state (“Pre-Quenched”) or towards a radio flare (“Pre-Flare”) that has always been observed after a quenched state: i.e., the γ -ray emission is detected when the system is moving into or out of a quenched state. So that, from a purely phenomenological point of view, the *quenched state* seems to be a “key” condition for the γ -ray emission.

Table 1: Main events of γ -ray activity ($\sqrt{TS} \gtrsim 3$) detected by the AGILE-GRID. *Column one:* date of the γ -ray event (average in MJD). *Column two:* X-ray spectral state. *Column three:* radio-flux-density state at the time of the γ -ray activity. *Column four:* time delay (ΔT_2) in days between the γ -ray event and the major radio flare. *Column five:* radio flux density of the major radio flare.

MJD	X-ray State	Radio State	ΔT_2 [days]	Radio flux density
54507.19	X-ray state trans. level	(?)	(?)	(?)
54573.08	Soft	Pre-Flare	~ 1	≈ 16 Jy (11.2 GHz)
54773.17	Soft	Pre-Quenched	~ 8	≈ 1 Jy (15 GHz)
54812.39	Soft	Pre-Flare	~ 6	≈ 3 Jy (11.2 GHz)
55003.37	Soft	Pre-Quenched	(?)	(?)
55025.55	Soft	Pre-Flare	~ 3	≈ 3 Jy (11.2 GHz)
55034.88	Soft	Pre-Flare	~ 1	≈ 2.3 Jy (11.2 GHz) ≈ 1.6 Jy (15 GHz)

We stress that in general γ -ray events – always during soft states – occur in proximity of spectral X-ray transitions. In particular we found that intense transient γ -ray emission is detected both immediately after hard-to-soft (e.g., the events of 2-3 November 2008 [MJD = 54773.17] and 20-21 June 2009 [MJD = 55003.37]) and before soft-to-hard spectral X-ray transitions (e.g., the events of 16-17 April 2008 [MJD = 54573.08], 11-12 December 2008 [MJD = 54812.39] and 13-14 July 2009 [MJD = 55025.55]). Observing Figure 1 and the zooms in Figure 2, we can note that strong transient γ -ray emission generally occurs when the system has just entered into or is moving out of a prominent minimum of the *Swift*/BAT light curve (e.g., November-December 2008 [MJD \approx 54770-54815] and June-July 2009 [MJD \approx 55000-55040] events.).

This comprehensive study confirms that the γ -ray emission conditions of Cygnus X-3, during the whole “pointing” monitoring by the AGILE satellite, are completely in agreement with the ones found by Tavani et al., 2009a; Bulgarelli et al., 2012a; Corbel et al., 2012.

3.2. Peculiarities of the gamma-ray events

3.2.1. The gamma-ray event of 11-12 February 2008 (MJD = 54507.19)

A more detailed discussion is needed for the γ -ray event of 11-12 February 2008 (MJD = 54507.19, see the upper-left panel in Figure 2), which is a special event among the AGILE-GRID detections.

The γ -ray activity in this period occurred when Cygnus X-3 was at the transitional level between soft and hard X-ray spectral state (*RXTE*/ASM count rate ~ 3 counts s⁻¹) and coincides with a short but sharp dip of the *Swift*/BAT light curve: MJD = 54508, count rate = (0.019 ± 0.005) counts cm⁻² s⁻¹, DATA_FLAG = 0 (data quality flag = good). Even if the event does not occur in coincidence with a *bright* soft state, it seems to confirm the simultaneous γ -ray-event/hard-X-ray-minimum occurrence that we find in all other cases. There are no available radio data for this period.

⁶ *Swift*/BAT (Burst Alert Telescope) transient monitor results provided by the *Swift*/BAT team.

⁷ *Rossi X-ray Timing Explorer* (RXTE), All-Sky Monitor (ASM). Quick-look results provided by the *RXTE*/ASM team.

⁸ Courtesy of the *Arcminute Microkelvin Imager* (AMI) Team.

⁹ Courtesy of S. Trushkin and the RATAN-600 Team.

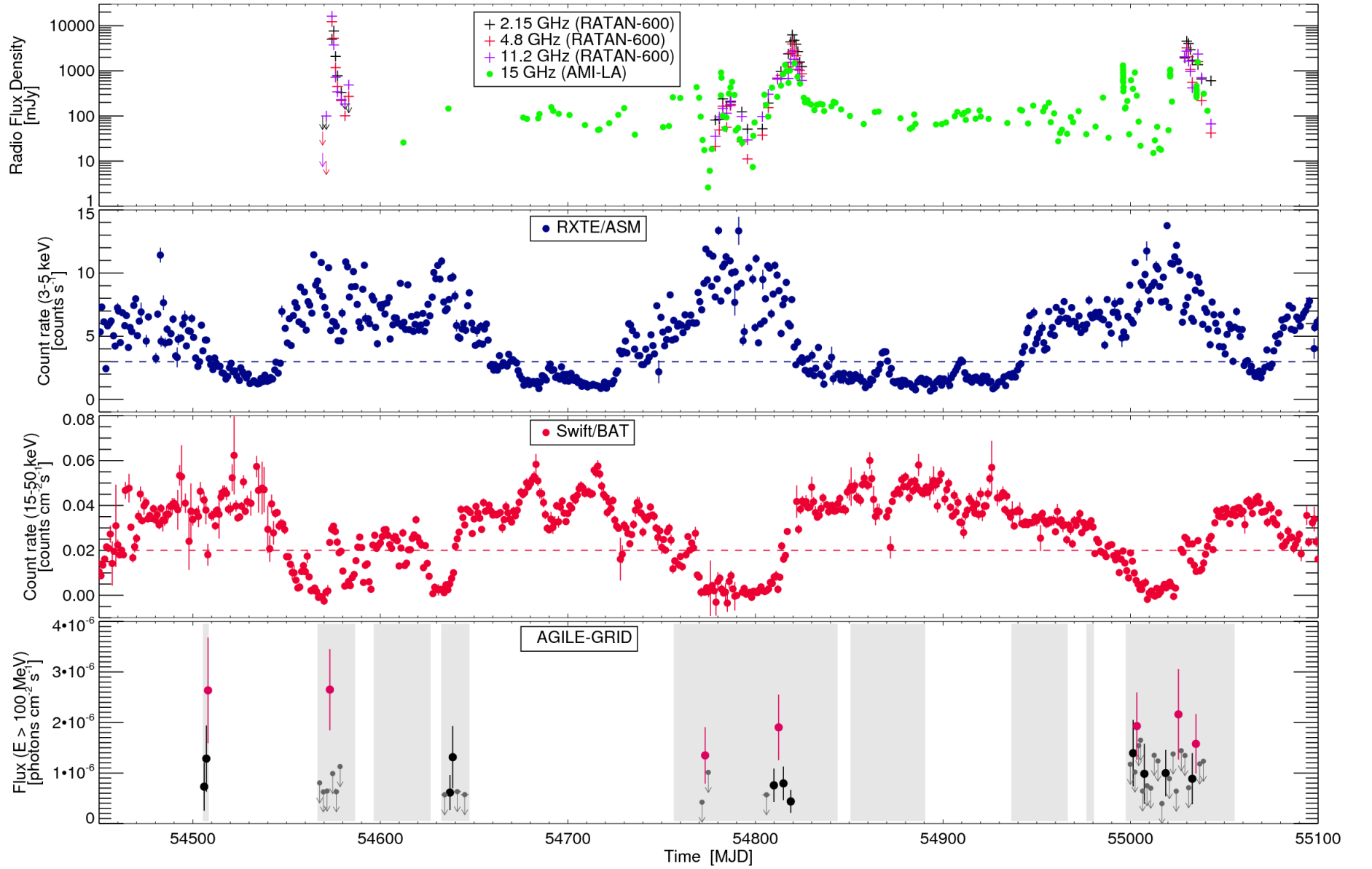


Fig. 1: Multi-frequency light curve of Cygnus X-3 from 2007-December-12 to 2009-September-26 (MJD: 54450-55100). From top to bottom: **radio** flux density [RATAN-600 (2.15, 4.8, 11.2 GHz) and AMI-LA (15 GHz)], **soft X-ray** count rate [RXTE/ASM (3-5 keV)], **hard X-ray** count rate [Swift/BAT (15-50 keV)] and **gamma-ray** photon fluxes [AGILE-GRID (above 100 MeV)]. In the bottom panel gray regions represent the AGILE pointing at the Cygnus region; *magenta* points are the main events of γ -ray activity with $\sqrt{TS} \geq 3$ (see Table A.1), *black* points are the γ -ray detections with $2 \leq \sqrt{TS} < 3$ and *dark-gray* arrows are the 2σ upper limits related to $\sqrt{TS} < 2$. The dashed lines in the panels of the RXTE/ASM and Swift/BAT count rate represent the transition level of 3 counts s⁻¹ and 0.02 counts cm⁻² s⁻¹ respectively (see Section 3.1 for details).

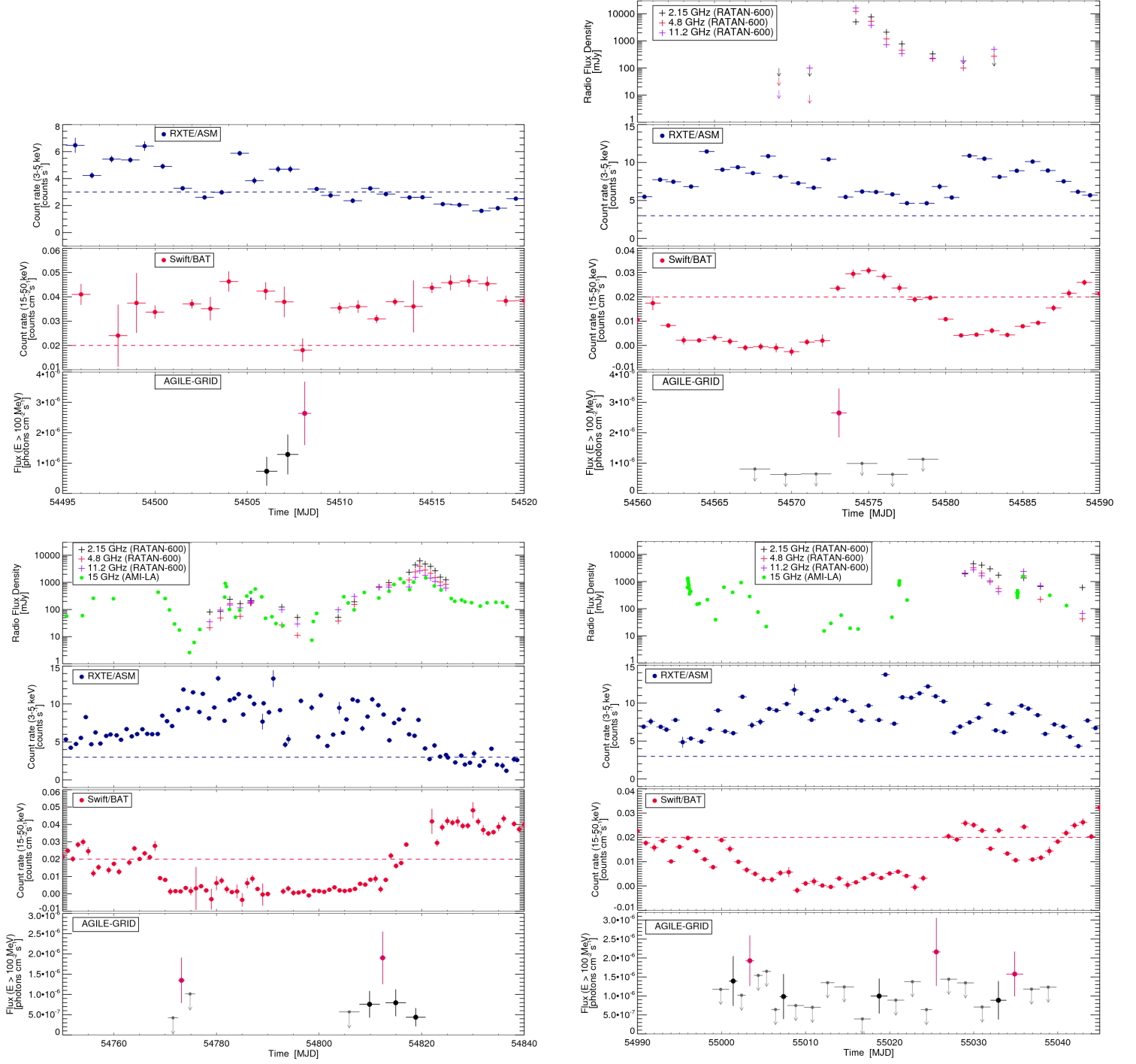


Fig. 2: Multi-frequency light curves centered on the main events of γ -ray activity detected by the AGILE-GRID (detailed views of the main plot in Figure 1). *Upper-left* plot: from 2008-January-30 to 2008-February-24 (MJD: 54495-54520). *Upper-right* plot: from 2008-April-04 to 2008-May-04 (MJD: 54560-54590). *Lower-left* plot: from 2008-October-11 to 2009-January-09 (MJD: 54750-54840). *Lower-right* plot: from 2009-June-08 to 2009-August-02 (MJD: 54990-55045).

3.2.2. The gamma-ray event of 20-21 June 2009 (MJD = 55003.37)

The γ -ray event on 20-21 June 2009 (MJD = 55003.37) occurred at the beginning of a quenched radio state (see the lower-right panel in Figure 2); unfortunately we have no subsequent radio data covering the following days (from the 3rd to the 9th day after the γ -ray event), but we cannot exclude the presence of a major radio flare – soon after the quenched state – that might have escaped detections. In Figure 2 (*Lower-right* panel) we note that the AMI-LA light curve (15 GHz) shows a following radio flare ~ 18 days after the γ -ray event (~ 13 days after the quenched state), possibly indicating a delayed radio burst (MJD = 55021.2, radio flux density = 1.06 Jy).

3.2.3. The long-term gamma-ray emission June-July 2009 (MJD \approx 55000-55040)

Finally, we note that the extended γ -ray activity of June-July 2009 (see the lower-right panel in Figure 2), occurred during an intense radio activity (with a high average radio flux density) coincident with a long-lasting soft X-ray spectral state. It is important to remark that this period coincides with one of the two temporal windows of strong γ -ray activity detected by *Fermi*-LAT, with a peak photon flux greater than $\sim 200 \times 10^{-8}$ photons $\text{cm}^{-2} \text{s}^{-1}$ (Abdo et al., 2009). This γ -ray peak is simultaneous (and consistent) with the event detected by the AGILE-GRID on 21-23 July 2009 (photon flux = $(158 \pm 59) \times 10^{-8}$ photons $\text{cm}^{-2} \text{s}^{-1}$). These data (June-July 2009) are discussed in more detail in a dedicated paper on the γ -ray emission of the microquasar during the mid-2009/mid-2010 period (Bulgarelli et al., 2012a).

4. Modeling the Spectral Energy Distribution

By accounting for the X-ray, γ -ray (AGILE-GRID) and TeV emission (MAGIC spectral upper limits), we modeled the multi-wavelength Spectral Energy Distribution (SED) of Cygnus X-3 during soft spectral state, with both *leptonic* and *hadronic* scenarios. We considered a X-ray spectrum measured by *RXTE*-PCA¹⁰ and *RXTE*-HEXTE¹¹ (~ 3 –150 keV) when the source was in a “hypersoft” state (Koljonen et al., 2010), the AGILE-GRID spectrum for the main γ -ray events (Figure A.1), and the MAGIC differential flux upper limits obtained when the source was in the soft state. (Aleksić et al., 2010). The hypersoft state of Cygnus X-3, subclass of the ultrasoft state defined in Hjalmarsdotter et al., 2009, is usually exhibited by the microquasar during the quenching/pre-flaring radio activity¹². This X-ray spectral state is characterized by a weak and hard power law tail ($\alpha = 1.7$ –1.9) with a non-thermal origin. Thus, we analyzed a pattern of multiwavelength datasets that, even if not simultaneous, are qualitatively consistent because they are all referred to the same spectral state of Cygnus X-3: the X-ray and AGILE-GRID datasets are related to the soft-state activity preceding the radio major flares, the TeV data are related to the soft-state activity following the radio major flares (MAGIC has never observed Cygnus X-3 during the pre-flaring radio states).

4.1. A leptonic scenario

We have modeled the multi-frequency SED by assuming a simple leptonic scenario: a plasmoid of high energy electrons/positrons, injected in the jet structure, that upscatters – via inverse Compton interactions – soft seed photons from the WR star and from the accretion disk.

Our aim is to analyze a possible link between the power law tail of this special soft X-ray spectral state and the γ -ray emission detected by the AGILE-GRID.

The physical parameters of the photon field are literature-based. We modeled the X-ray data with a black body (BB) spectrum¹³ characterized by a $T_{bb} \approx 1.3$ keV (consistent with the typical value of the characteristic temperature of the disk during the hypersoft/ultrasoft state: Hjalmarsdotter et al., 2009; Koljonen et al., 2010) and a $L_{bb} \approx 8 \times 10^{37}$ erg s^{-1} . The main parameters we used for the WR star are: $T_\star = 10^5$ K, $L_\star \approx 10^{39}$ erg s^{-1} (see Dubus et al., 2010). The WR star is assumed to emit UV photons isotropically. We modeled the average γ -ray emission in the orbital phase, so we assumed the seed photons from the companion star colliding with the leptons mainly on the side of the jet.

We have carried out two different models: in the first one (leptonic model “A”) the plasmoid interacts with the soft photon bath “close” to the disk (the star-plasmoid distance is $R \approx d \approx 3 \times 10^{11}$ cm), in the second one (leptonic model “B”) the interaction region is “far away” from the accretion disk (the star-plasmoid distance is $R \approx 10d \approx 3 \times 10^{12}$ cm). For both models, the inclination of the jet to the line of sight is assumed to be $i = 14^\circ$, and the plasmoid is assumed to be spherical (radius $r = 3 \times 10^{10}$ cm) with a bulk motion characterized by a Lorentz factor of $\Gamma = 1.5$ ($v = \sqrt{5}c/3$). The population of electrons is modeled by a broken-power-law spectral distribution, with spectral indices $\alpha_1 = 2.2$, $\alpha_2 = 4.0$, $\gamma_{min} = 1$, $\gamma_{max} = 10^5$ and energy break of $\gamma_b = 4 \times 10^3$:

$$\frac{dN}{d\gamma dV} = \frac{K_e \gamma_b^{-1}}{\left(\frac{\gamma}{\gamma_b}\right)^{\alpha_1} + \left(\frac{\gamma}{\gamma_b}\right)^{\alpha_2}} \quad [\gamma_{min} \leq \gamma \leq \gamma_{max}] \quad (1)$$

The spectral indices and the energy break of the electron distribution are the best-fitting values on the AGILE-GRID spectral shape. The distribution of electrons/positrons is assumed to be isotropic in the plasmoid rest frame (the jet comoving frame). We adopted the Klein-Nishina formula to describe the Compton scattering of soft photons by a cloud of mildly relativistic leptons (Aharonian & Atoyan, 1981).

In the leptonic model “A” the distance from the star to the plasmoid location is assumed to be $R \approx 3 \times 10^{11}$ cm ($R \approx d$), i.e., the plasmoid in the jet is very close to the compact object and to the accretion disk. The distance between the plasmoid center and the compact object is $H \approx 3 \times 10^{10}$ cm, i.e., $H \approx r$. The result of this modeling is in Figure 3. The electron number density of the plasmoid is $n_e \approx 3 \times 10^9$ electrons cm^{-3} (the prefactor K_e in Eq. (1) is $K_e = 2 \times 10^5 \text{ cm}^{-3}$, the integrated number of electrons is $N_e = 3 \times 10^{41}$). We took into account the $\gamma\gamma$ absorption (for e^\pm pair production) between the X-ray photons

¹⁰ Proportional Counter Array (PCA)

¹¹ High Energy X-ray Timing Experiment (HEXTE)

¹² This is an average “hypersoft” spectrum related to 28 pointed *RXTE* observation between February 2000 and January 2006 (see the Supporting Information of Koljonen et al., 2010 for details).

¹³ Our modeling is a simplification: we are assuming that the bump in the X-ray emission during the “hypersoft” state can be modeled with a simple BB component, that is a very good approximation for our purpose. In this state the overall X-ray emission is totally dominated by a strong BB emission from the accretion disk. Nevertheless, a more accurate modeling should be based on a Comptonized BB spectrum by the corona (see Koljonen et al., 2010 for details).

from disk and the IC γ -rays photons. We assumed that the distribution of the disk photons is fully isotropized by the stellar wind in the observer frame. This implies that the γ -ray photosphere (i.e., where $\tau_{\gamma\gamma} \geq 1$) has a radius of $\sim 10^{10}$ cm (Cerutti et al., 2011). With these assumptions, the lowest part of the plasmoid is within the γ -ray photosphere¹⁴. The spectral component related to IC scatterings on the disk photons (green curve) is actually produced in this region, very close to the disk, where the X-ray photon density as well as the optical depth is high. Since $\tau_{\gamma\gamma} > 1$, this component shows a sharp cut-off at ~ 100 MeV (i.e., the threshold for e^\pm production, given the characteristic energies of the disk photons). On the other hand, the spectral component related to IC scatterings on the stellar wind photons (red curve) does not show any cut-off, because it is mainly produced in the farthest part of the plasmoid (outside the γ -ray photosphere, for distances greater than $\sim 10^{10}$ cm with respect to the disk), where the $\gamma\gamma$ absorption by the X-ray disk photons is negligible. Thus, we deduce that in our geometry the plasmoid volume outside the γ -ray photosphere emits the bulk of the γ -ray emission above 100 MeV via IC processes on stellar photons (see Figure 3). In model “A”, assuming a lepton injection rate of $\dot{N}_e = n_e \pi r^2 v \approx 2 \times 10^{41}$ leptons s^{-1} , the jet kinetic luminosity for the leptons ($L_{kin, e} = \dot{N}_e \Gamma m_e c^2$) would be $L_{kin, e}^A \approx 2 \times 10^{35}$ erg s^{-1} .

In the leptonic model “B” the distance from the star to the plasmoid is assumed to be $R \approx 3 \times 10^{12}$ cm ($R \approx 10d$), i.e., the plasmoid in the jet is far away from the compact object and the accretion disk. The distance between the plasmoid center and the compact object is $H \approx 3 \times 10^{12}$ cm, i.e., $R \approx H$. We assumed that the disk photons are entering in the plasmoid mainly from behind. The results of this modeling are shown in Figure 4. The electron density of the plasmoid is $n_e \approx 1.5 \times 10^{11}$ electrons cm^{-3} (the prefactor K_e in Eq. (1) is $K_e = 8 \times 10^6$ cm^{-3} , the integrated number of electrons is $N_e = 1.5 \times 10^{43}$). In this model the spectral component related to the IC scatterings on disk photons (green curve) is negligible compared to the IC component on soft photons from the star (red curve). We remark that the “IC disk” component does not show any cut-off related to $\gamma\gamma$ absorption by X-ray photons, because the IC γ -rays are produced well outside the γ -ray photosphere (at distances $\gg 10^{10}$ cm). In model “B”, assuming a lepton injection rate of $\dot{N}_e = n_e \pi r^2 v \approx 10^{43}$ leptons s^{-1} , the jet kinetic luminosity for the leptons ($L_{kin, e} = \dot{N}_e \Gamma m_e c^2$) would be $L_{kin, e}^B \approx 10^{37}$ erg s^{-1} .

In these models, the expected VHE γ -ray emission would be very faint. These expectations are consistent with the MAGIC upper limits, and might explain the lack of TeV bright detections during soft states.

4.2. A hadronic scenario

We also considered a “hadronic scenario” for γ -ray production from Cygnus X-3. In our model we used the same formalism adopted by Romero et al. (2003). In this case, the compact source is assumed to eject a flux of mildly relativistic hadrons (mostly protons) at the base of the jet. These protons are first accelerated near the compact object and then propagate along the jet interacting with the gaseous surroundings provided by the WR companion mass outflow. The resulting proton-proton (pp) collisions can copiously produce pions and γ -rays resulting from neutral pion decays.

The proton distribution in the jet is assumed to be isotropic in the jet comoving frame, with an energy spectrum described by a power law with a high energy cut-off:

$$\frac{dN}{dydV} = K_p \gamma^{-\alpha} \exp(-\gamma/\gamma_c) \quad [\gamma \geq \gamma_{min}] \quad (2)$$

with $\alpha = 3$, $\gamma_{min} = 1$ and $\gamma_c = 100$. The spectral index of the distribution is the best-fitting value on the AGILE-GRID spectral shape. We set the energy cut-off value at $\gamma_c = 100$ so that the total SED is consistent with the spectral constraints of the MAGIC upper limits.

The ejected protons interact with the hadronic matter of the WR strong wind. The inelastic hadronic scatterings produce neutral pions that subsequently decay in γ -rays. We adopted the same formula for the cross section $\sigma_{pp}(\gamma)$ for inelastic pp interaction reported by Kelner et al. (2006). We assumed that the injected protons in the jet interact with the gas of the wind along a cylindrical column of matter¹⁵ with a radius $r = 3 \times 10^{10}$ cm and a height of $H \approx 3 \times 10^{12}$ cm (this height provides the interesting part of the cylinder in which most of the interactions take place). In analogy with the leptonic models, we assumed for the jet a bulk Lorentz factor of $\Gamma = 1.5$, and an inclination to the line of sight of $i = 14^\circ$. In order to quantify the density of matter in the WR wind, we assumed that the companion star has a mass loss rate of $\dot{M} \sim 10^{-5} M_\odot$ yr^{-1} and the speed of the wind is $v_{wind} \sim 1000$ km s^{-1} (Szostek & Zdziarski, 2008). By integrating the density of matter in this cylinder expressed in terms of number density of protons ($\rho \sim 1/R^2$, where R is the distance from the star), we find that the total number of protons from the wind in this column is $N_{p, wind} \approx 3.7 \times 10^{45}$.

We considered a variety of proton injection rates in the jet, $\dot{N}_{p, jet}$. The result of our best hadronic model for Cygnus X-3 is reported in Figure 5. In this case, the integrated number of protons injected in the jet is $N_{p, jet} \approx 9.0 \times 10^{42}$, and the average number proton density in the column of interest is $n_{p, jet} \approx 1.1 \times 10^9$ protons cm^{-3} .

The proton injection flux in the jet of our best model turns out to be $\phi_{p, jet} \approx 2.4 \times 10^{19}$ protons $cm^{-2} s^{-1}$, that corresponds to a proton injection rate of $\dot{N}_{p, jet} \approx 6.7 \times 10^{40}$ protons s^{-1} .

In Cygnus X-3 the corresponding jet kinetic luminosity for the hadrons ($L_{kin, p} = \dot{N}_p \Gamma m_p c^2$) would be $L_{kin, p} \approx 1.5 \times 10^{38}$ erg s^{-1} . This value is consistent with the average bolometric luminosity of the hypersoft state, $L_{bol}^{HYS} \approx 1.2 \times 10^{38}$ erg s^{-1} (Koljonen et al., 2010). Moreover, $L_{kin, p}$ is lower than the Eddington accretion limit for the system, that is $L_{Edd} \approx 10^{39}$ erg s^{-1} , assuming that the compact object is a black hole with a mass of $M_x \approx 10 M_\odot$.

5. Discussion

In the context of a leptonic scenario, we find that most of the γ -ray emission above 100 MeV is due to IC scatterings on wind stellar photons (see Figures 3 and 4), according to the results of Dubus et al., 2010 and Zdziarski et al., 2012. We remark that the IC cooling times are very short ($t_{IC} \sim 1$ – 10 s). Thus, the observed time scale of γ -ray emission (1–2 days) and the strong orbital modulation (~ 4.8 hours) detected in γ -rays (Abdo et al., 2009) impose a continuous injection of accelerated particle in the jet. The γ -ray emission, as remarked also by Zdziarski et al. (2012),

¹⁴ Assuming that the photosphere radius is equal to the plasmoid radius, i.e., 3×10^{10} cm, the fraction of the plasmoid volume inside the γ -ray photosphere is $\sim 32\%$.

¹⁵ A cylindrical configuration of the jet corresponds to set $\epsilon = 0$ in the formalism adopted by Romero et al. (2003) to describe the jet radius dependence on the axis, $r(z) = \xi z^\epsilon$.

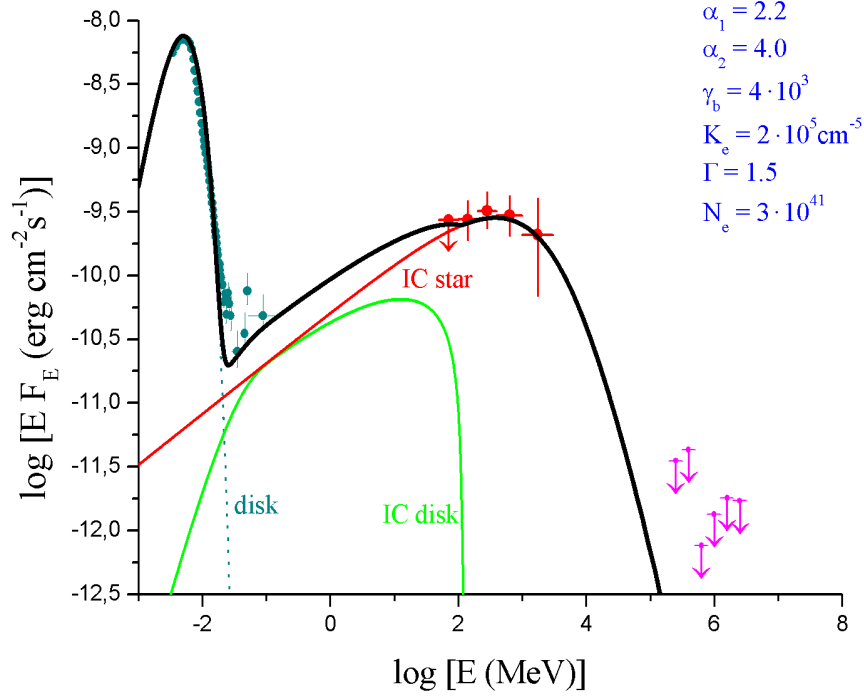


Fig. 3: Multiwavelength SED of Cygnus X-3 during the main γ -ray events (non-simultaneous data), leptonic model “A” (see main text). *Blue circles*: X-ray average “hypersoft” spectrum (Koljonen et al., 2010), *RXTE*-PCA and *RXTE*-HEXTE data (~ 3 to ~ 150 keV); *red circles*: AGILE-GRID energy spectrum (50 MeV to 3 GeV) of the main γ -ray episodes (Figure A.1 and A.2); *magenta arrows*: MAGIC differential flux upper limits (95% C.L.), 199–3155 GeV, related to soft spectral state (Aleksić et al., 2010). Spectral components of the model: black body (BB) emission from disk (blue short-dashed line), Inverse Compton (IC) on soft photons of the accretion disk (green solid line), Inverse Compton (IC) on soft photons of the stellar wind (red solid line). Global SED model curve in black solid line.

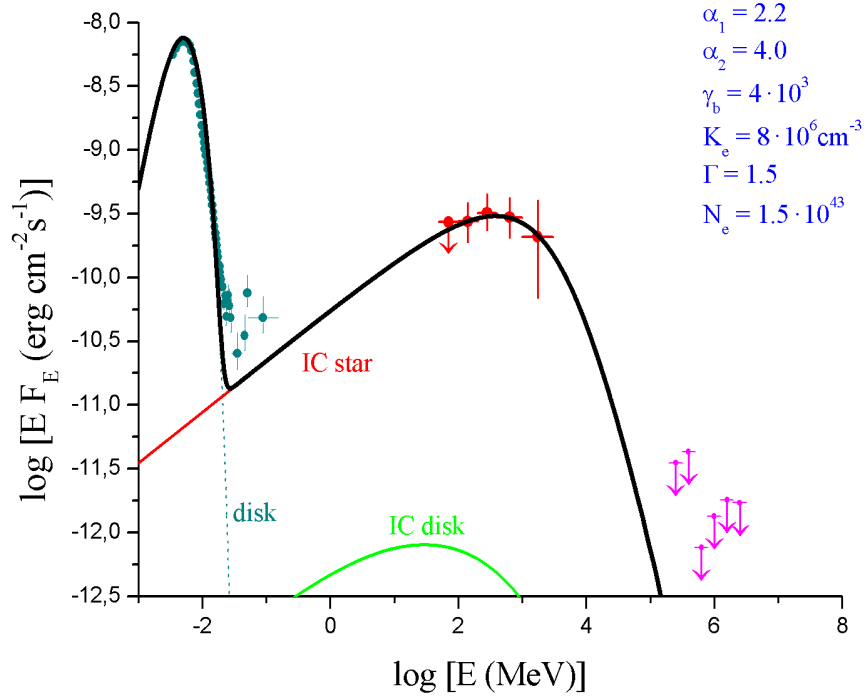


Fig. 4: Multiwavelength SED of Cygnus X-3 during the main γ -ray events (non-simultaneous data), leptonic model “B” (see main text). Spectral components of the model: BB emission from disk (blue short-dashed line), Inverse Compton (IC) on soft photons of the accretion disk (green solid line), Inverse Compton (IC) on soft photons of the stellar wind (red solid line). Global SED model curve in black solid line. For a detailed description of the datasets, see caption in Figure 3.

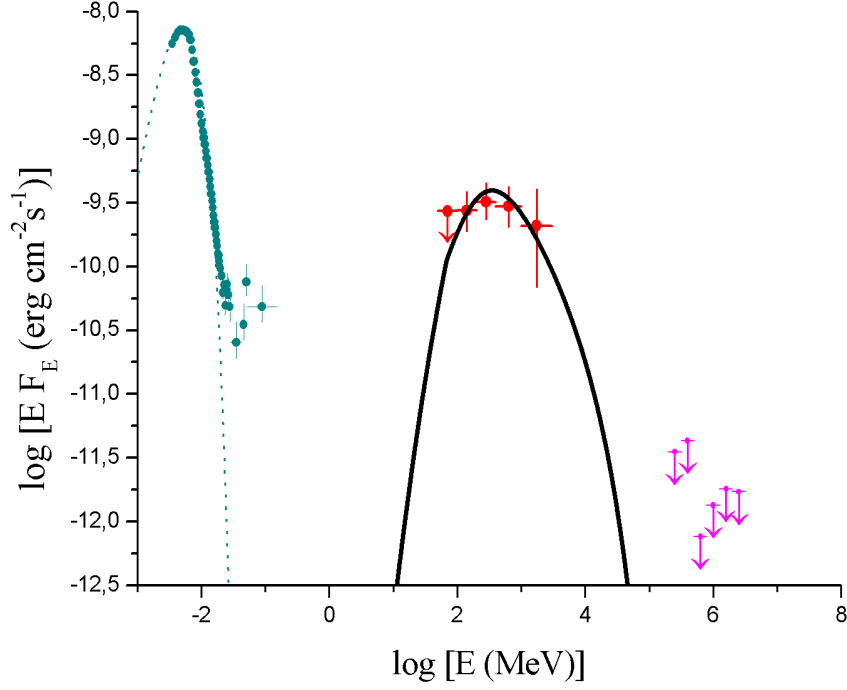


Fig. 5: Multiwavelength SED of Cygnus X-3 during γ -ray events (non-simultaneous data), hadronic model (see main text). BB emission from disk (blue short-dashed line), γ -ray emission from π^0 -decays (black solid line). For a detailed description of the datasets, see caption in Figure 3.

cannot be related to a single injection of a relativistic plasmoid in the jet. Our leptonic picture could suggest a substructure. We find that the innermost part of the jet, where the density of X-ray disk photons is high, could give a strong contribution to the hard X-rays at ~ 100 keV. In model “A”, the spectral component related to IC scatterings on soft photons from the disk (green curve) gives a substantial contribution to the overall model below ~ 100 MeV that is consistent with the hard tail of the X-ray dataset (see Figure 3). This model suggests a possible spectral link between the power-law tail of ultrasoft/hypersoft state and the γ -ray emission detected by the AGILE-GRID. On the other hand, in the region of the jet outside the γ -ray photosphere related to pair production on disk photons ($H \gtrsim 10^{10}$ cm), the “IC disk” component becomes very low at ~ 100 keV and the overall contribution to the hard X-rays is negligible (Figure 4). Thus, according to model “B”, if the region of γ -ray emission is far away from the compact object, the power-law tail in the hard X-ray band cannot be accounted for by IC processes in the jet. For this reason we assumed two “extreme” cases in the spatial configuration of the γ -ray emitting blob, that is located at $H \approx 3 \times 10^{10}$ cm (model “A”), and at $H \approx 3 \times 10^{12}$ cm (model “B”). Dubus et al. (2010) found that the γ -ray emitting region is located at a distance $H \lesssim 10d \approx 3 \times 10^{12}$ cm. By assuming that the compact object is a black hole with a mass of $M_x = 20M_\odot$, their simulation give the best fit of the γ -ray modulation for $H \approx 3 \times 10^{11}$ cm. So that, the bulk of the γ -ray emission is possibly produced at an intermediate configuration between models “A” and “B”. The leptonic picture “B” is qualitatively consistent with the one proposed by Zdziarski et al. (2012) to explain the Fermi-LAT data published in Abdo et al. (2009), even if the peak energy of the IC bump is quite different: in our models the peak energy is between ~ 100 MeV and ~ 1 GeV, in their models the peak energy is between ~ 3 and ~ 50 MeV. This difference could be due to the unequal spectral indices of the γ -ray spectra detected by the

AGILE-GRID and by Fermi-LAT (see Figure A.2). Moreover, Zdziarski et al. (2012) assumed that the electrons are injected in the jet with a power-law rate for $\gamma_1 \leq \gamma \leq \gamma_2$. The electrons subsequently lose energy via Compton, synchrotron and adiabatic losses and form a distribution below γ_1 . Thus, they demonstrated that models with $\gamma_1 < 10^3$ give strong contribution to the hard X-rays, which appears in conflict with the observed orbital modulation at ~ 100 keV during the γ -ray emitting intervals, that is out of phase with the γ -ray modulation at > 100 MeV (Zdziarski et al., in press). This phase misalignment would rule out any substantial contribution of the jet to the hard X-rays, in (apparent) contradiction with our findings in model “A”. First, we remark that in our models the energy distributions of the accelerated particles are assumed to be “steady-state” spectra, subsequent to physical cooling processes, and not injected spectra. Then, our leptonic models are based on IC scatterings on both UV stellar photons and X-ray disk photons, whereas Zdziarski et al. (2012) consider the UV stellar photons only (neglecting the X-ray photons from the accretion disk). By observing Figure 3, we note that at ~ 100 keV the contribution of the “IC disk” component (green curve) is equivalent to the contribution of the “IC star” component (red curve). But, if the latter has a modulated emission (the jet-wind geometry is anisotropic during the orbital phase), the former would not change with the orbital period (the jet-disk geometry should not significantly change with orbital phase). Thus, the effective unabsorbed modulation at ~ 100 keV – that is a superposition of a modulated and a unmodulated component – should have a lower amplitude with respect to the effective modulation at energies > 100 MeV – that is actually related to the modulated “IC star” component only. Moreover, anisotropic absorption effects in the wind could strongly affect the unabsorbed 100 keV emission and produce an observed modulation in phase with the soft X-ray band.

Finally, we remark that, for energies greater than ~ 10 GeV, γ -

rays are above the threshold for pair production on stellar photons. Nevertheless, [Zdziarski et al., 2012](#) demonstrated that, for a similar choice of geometrical parameters, the value of the optical depth is moderate and peaks at ~ 0.1 – 1 TeV. Thus, the $\gamma\gamma$ absorption by UV stellar has been neglected in our (leptonic and hadronic) models.

In the context of a hadronic scenario, we use a model similar to the one proposed by [Romero et al. \(2003\)](#). The only substantial difference consists in the jet geometry: we use a cylindrical model, whereas they use a conical configuration. We found that a simply hadronic model can account for the γ -ray spectrum detected by the AGILE-GRID, by assuming a reasonable proton injection rate in the jet. It is interesting to compare our best-fit hadronic injection rate for Cygnus X-3 with the value deduced for the microquasar SS433 that is known to produce a quasi-steady jet of hadronic nature ([Migliari et al., 2002](#)). SS433 is characterized by a hadronic jet mass ejection rates near $\dot{M}_{jet} \approx 5 \times 10^{-7} M_{\odot} \text{ yr}^{-1}$ ([Konigl, 1983](#); [Fabrika & Borisov, 1987](#); [Reynoso et al., 2008](#)), that corresponds to a proton injection rate of $\dot{N}_{p,jet}^{SS433} \approx 1.9 \times 10^{43} \text{ protons s}^{-1}$. Thus, we have that $\dot{N}_{p,jet}^{Cyg-X-3} \approx 3.5 \times 10^{-3} \dot{N}_{p,jet}^{SS433}$. SS433 ejects hadrons in a quasi-steady fashion, Cygnus X-3 ejects hadrons in highly variable regime with a lower injection rate.

Our hypothesis for a hadronic interpretation of γ -ray emission from Cygnus X-3 needs to be supported by information that at the moment is not yet available, such as hadronic emission lines in the flare spectra, and a precise characterization of the γ -ray spectrum at energies below 100 MeV that should show the characteristic decrement of neutral pion emission. Furthermore, hadronic mechanisms, besides emitting strong γ -ray radiation via π^0 -decay, would produce intense flux of high-energy neutrinos, emerging from the decay of secondary charged mesons produced in pp collisions. So, a firm simultaneous detection of strong neutrino flux and γ -ray activity from Cygnus X-3, would represent the signature of a dominant hadronic mechanism in the relativistic jet.

In this scenario, considering the temporal coincidence of γ -ray/radio flares, we are implicitly assuming that the hadronic component of the jet provides the main contribution to the γ -ray emission, and the leptonic component produces – via synchrotron emission process – the strong radio flares far away from the compact object. In addition to γ -rays from π^0 -decays, hadronic pp interactions are expected to produce a population of secondary electrons (and positrons) from the decay of charged pions (π^{\pm}). These secondary leptons can contribute to the emission in the radio band via synchrotron processes and in γ -rays (marginally with respect to the contribution by π^0 -decay) via IC and Bremsstrahlung processes.

6. Conclusions

Several events of γ -ray activity were detected by the AGILE-GRID from Cygnus X-3 while the system was in a special radio/X-ray spectral state: intense γ -ray activity was detected always during prominent minima of the hard X-ray light curve (corresponding to strong soft X-ray emission), a few days before intense radio outbursts (major radio flares). This temporal repetitive coincidence turns out to be the spectral signature of the γ -ray activity from this puzzling microquasar, and might open new areas to study the interplay between the accretion disk, the corona and the formation of relativistic jets. The simultaneous strong soft X-ray emission from the disk and γ -ray emission from the jet preceding intense radio outbursts might suggest a

scenario in which the hot thermal corona “dissolves”, and the accretion power from the disk directly charges the jet, that then emits γ -rays and, subsequently, radio outbursts (via synchrotron processes) far from the compact object.

The γ -ray detections of Cygnus X-3 imply new constraints to the emission models for such powerful X-ray binary, indicating that hybrid-Comptonization mechanisms ([Coppi, 1999](#)) alone cannot account for the γ -ray fluxes detected by AGILE and Fermi above 100 MeV, unless we assume unrealistic physical parameters ([Cerutti et al., 2011](#)). This implies that the corona cannot be the site of γ -ray emission. We found that the innermost part of the jet (distances $\lesssim 10^{10}$ cm from the compact object) could give a strong contribution to the hard X-rays at ~ 100 keV during the γ -ray emitting interval, while the farthest part (distances $\gtrsim 10^{10}$ cm from the compact object) produces the bulk of the γ -ray emission above 100 MeV.

We found that the γ -ray spectrum of Cygnus X-3 detected by the AGILE-GRID is significantly harder than the time averaged spectrum obtained by Fermi-LAT for the “ γ -ray active periods” of the microquasar, lasting ~ 4 months (see Figure A.2). Although both the AGILE main γ -ray events and the Fermi γ -ray active periods are both likely related to the presence of an active jet, the spectral difference may imply a fast hardening of the spectrum during the peak γ -ray events, lasting ~ 1 – 2 days.

We have demonstrated that both a leptonic model based on inverse Compton emission from a relativistic plasmoid injected in the jet and a hadronic model based on π^0 -decays, might account for the γ -ray emission observed by the AGILE-GRID. Both these models require the introduction of a new component (“IC bump” or “ π^0 -bump”) in the SED of the system.

A leptonic scenario seems to be more likely than a hadronic one: the γ -ray modulation, the spectral link between hard X-ray and γ -ray spectra, the temporal link between γ -ray events and radio flares could be interpreted in a natural way by assuming that the electrons are the main emitters. According to our results, the γ -ray emission occurs within $\sim 10^{12}$ cm from the compact object. Interpreting as the propagation time of the relativistic jet ($v = \sqrt{5}c/3$) the ~ 4 -day delay between the onset of γ -ray and radio flaring emission, the radio burst would occur at a distance of $\sim 8 \times 10^{15}$ cm.

Our hadronic model, with the assumption of a standard WR wind, would require a jet kinetic power of $L_{kin, p} \approx 1.5 \times 10^{38} \text{ erg s}^{-1}$ to explain the γ -ray emission detected by AGILE. This value is of the same order of magnitude as the bolometric luminosity of the disk/corona during the hypersoft spectral state, and it is lower than the Eddington accretion limit for a black hole with a mass of $M_x \approx 10 M_{\odot}$ ($L_{Edd} \approx 10^{39} \text{ erg s}^{-1}$). So that, a hadronic picture is physically reasonable and not energetically disfavored with respect to a leptonic one. At present, there is no strong evidence for excluding one of these hypotheses, and it remains an open question whether the dominant process for γ -ray emission in microquasars is hadronic or leptonic ([Mirabel, 2012](#)).

The firm discovery of γ -ray emission from this microquasar represents the experimental proof that these astrophysical objects are capable of accelerating particles up to relativistic energies, through a mechanism – related to the disk-corona dynamics – that leads to jet formation.

Acknowledgements. The authors are grateful to the anonymous referee for her/his stimulating comments on the manuscript.

This investigation was carried out with partial support under ASI contracts nos. I/089/06/2, and I/042/10/0.

Appendix A: The AGILE-GRID dataset

We performed an analysis on the whole AGILE-GRID data in the period November 2007 - July 2009, using a detection algorithm that was developed by the AGILE Team to automatically search for transient γ -ray emission. The algorithm initially analyzed 140 maps, each related to a 2-day integration (non-overlapping consecutive time intervals). The time bins of peak γ -ray emission, with significance of detection greater than 3 sigma, have been found. The analysis was subsequently manually refined in order to optimize the determination of the time interval of the γ -ray emission. The whole analysis was carried out with the Build 19 version of the AGILE team software, using the FM3.119.2 calibrated filter applied on the consolidated dataset with off-axis angles less than 40° . We used a Multi-Source maximum-Likelihood Analysis (MSLA) to take into account the emission of the nearby γ -ray pulsars¹⁶: 1AGL J2021+3652 (PSR J2021+3651), 1AGL J2022+4032 (PSR J2021+4026), 1AGL J2032+4102 (PSR J2032+4127). In particular the MSLA is fundamental in order to avoid contamination by the pulsar PSR J2032+4127, located at a distance of $\sim 0.5^\circ$. In this paper we did not consider the off-pulse data for the nearby pulsar. Nevertheless, the MSLA accounted for the steady γ -ray emission from this source in the calculation of the significance and the flux of each γ -ray detection of Cygnus X-3. Moreover, we can exclude any substantial spectral contamination from the pulsar because the steady γ -ray emission from the pulsar¹⁷ is much smaller than the mean flux of the active γ -ray emission from Cygnus X-3.

The main events of γ -ray activity, detected with a significance above 3σ ($\sqrt{TS} \geq 3$), are shown in Table A.1. We found seven events¹⁸, including those presented in Tavani et al. (2009a) and in Bulgarelli et al. (2012a).

By integrating all the main events with FM3.119.2 filter, we found a γ -ray source detected at 6.7σ ($\sqrt{TS} = 6.7$) at the average Galactic coordinate (l, b) = $(79.7^\circ, 0.9^\circ) \pm 0.4^\circ$ (stat) $\pm 0.1^\circ$ (syst), with a photon flux of $(158 \pm 29) \times 10^{-8}$ photons $\text{cm}^{-2} \text{s}^{-1}$ above 100 MeV¹⁹. The average differential spectrum between 100 MeV and 3 GeV is well fitted by a power law with a photon index $\alpha = 2.0 \pm 0.2$ (Figure A.1). This value is consistent with the Cygnus X-3 photon index found by Tavani et al. (2009a) and Bulgarelli et al. (2012a). In Figure A.2 we present a comparison between the νF_ν spectra of Cygnus X-3 as detected by the AGILE-GRID and by Fermi-LAT (Abdo et al., 2009) during the γ -ray activity. It should be noted that the AGILE-GRID spectrum is related to the peak γ -ray activity only (the seven main events, lasting 1-2 days, in Table A.1), instead the Fermi-LAT

spectrum is an average spectrum detected during the two active windows (2 months each) of γ -ray emission from Cygnus X-3 (MJD: 54750–54820 and MJD: 54990–55045).

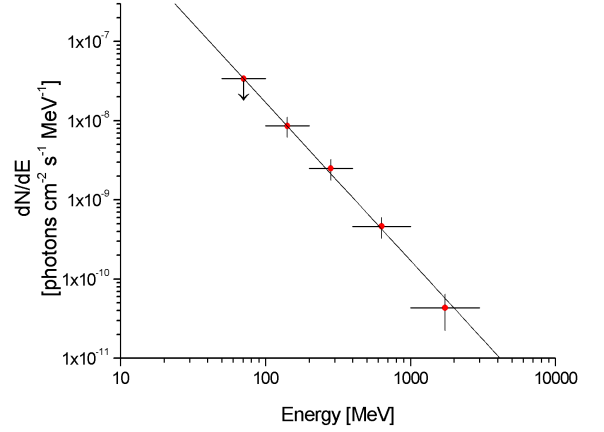


Fig. A.1: Photon spectrum between 50 MeV and 3 GeV of Cygnus X-3 as detected by the AGILE-GRID by integrating all the main γ -ray episodes in Table A.1. Power law fit on γ -ray data between 100 MeV and 3 GeV with photon index $\alpha = 2.0 \pm 0.2$.

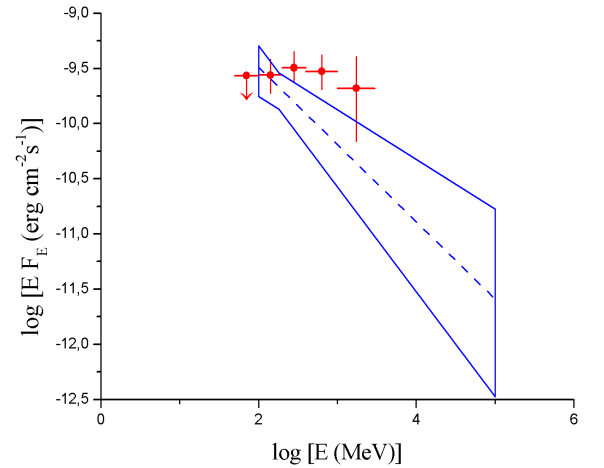


Fig. A.2: νF_ν spectra of Cygnus X-3 during the γ -ray activity. Red circles: AGILE-GRID energy spectrum (50 MeV to 3 GeV) of the main episodes (Figure A.1). Blue error contours and dashed blue line: average power-law fit with $\alpha = 2.70 \pm 0.25$ of the spectrum detected by Fermi-LAT during long integration (~ 4 months) in the active periods (Abdo et al., 2009).

¹⁶ The main characteristics of the persistent γ -ray sources we used in the MSLA are reported in the Table 1 of Chen, Piano et al. (2011)

¹⁷ The steady γ -ray emission from the pulsar PSR J2032+4127, as detected by the AGILE-GRID, is $F_\gamma^{PSR} = [37 \pm 4(\text{stat}) \pm 10\%(syst)] \times 10^{-8}$ photons $\text{cm}^{-2} \text{s}^{-1}$ for photon energy above 100 MeV, see Chen, Piano et al. (2011) for details.

¹⁸ All the γ -ray events were detected by using the same filter, FM3.119.2. As discussed in the Supplementary Information of Tavani et al. (2009a), the event of 2-3 November 2008 appears to be relatively “soft” in γ -rays compared to the other episodes. In fact, by analyzing the event with the FT3ab.2 filter (more efficient in detecting such kind of emission), we found a more significant detection: $\sqrt{TS} = 3.9$, photon flux above 100 MeV: $(214 \pm 73) \times 10^{-8}$ photons $\text{cm}^{-2} \text{s}^{-1}$.

¹⁹ Here we present an updated result for the analysis of the 7-events integration with respect to the one reported in Piano et al. (2011). In this paper the analysis has been carried out with a more recent version of the AGILE software tool (AG_multi4).

Finally, we evaluated the post-trial significance for repeated flare occurrences by using the same formalism of Bulgarelli et al. (2012b). The probability of having k or more detections – consistent with the position of Cygnus X-3 – with $\sqrt{TS} \geq \sqrt{h}$ in N trials, is:

$$P(N, k) = 1 - \sum_{j=0}^{k-1} \binom{N}{j} p^j (1-p)^{N-j}$$

where p is the p -value corresponding to h . For $\sqrt{TS} \geq 3$ we have a p -value of $p = 2.0 \times 10^{-3}$. So, for $N = 140$ (our trials, the number of 2-day integration maps analyzed by the initial

Table A.1: Main events of γ -ray emission detected by the AGILE-GRID in the period November 2007 - July 2009. All detections have a significance above 3σ ($\sqrt{TS} \geq 3$). *Column one:* period of detection in UTC; *Column two:* period of detection in MJD; *Column three:* significance of detection; *Column four:* photon flux (above 100 MeV).

Period	MJD	\sqrt{TS}	Flux [10^{-8} photons $\text{cm}^{-2} \text{s}^{-1}$]
2008-02-11 (18:07:28) - 2008-02-12 (11:07:44)	54507.76 - 54508.46	3.7	264 ± 104
2008-04-16 (13:59:12) - 2008-04-17 (13:48:00)	54572.58 - 54573.58	4.5	265 ± 80
2008-11-02 (13:01:05) - 2008-11-03 (19:01:05)	54772.54 - 54773.79	3.1	135 ± 56
2008-12-11 (19:50:40) - 2008-12-12 (23:02:40)	54811.83 - 54812.96	4.0	190 ± 65
2009-06-20 (21:04:48) - 2009-06-21 (20:53:04)	55002.88 - 55003.87	3.8	193 ± 67
2009-07-13 (01:11:60) - 2009-07-14 (00:59:44)	55025.05 - 55026.04	3.2	216 ± 89
2009-07-21 (21:07:12) - 2009-07-23 (21:07:12)	55033.88 - 55035.88	3.6	158 ± 59

algorithm) and $k = 7$ (our detections of Cygnus X-3), we found $P(140, 7) = 1.8 \times 10^{-8}$, that corresponds to 5.5 Gaussian standard deviations.

A Multi-Source maximum-Likelihood Analysis (MSLA), applied in the deep integration of the AGILE-GRID data (between November 2007 and July 2009), found a weak persistent emission (significance: $\sqrt{TS} = 5.17$) from a position consistent with Cygnus X-3²⁰ with a photon flux of $(14 \pm 3) \times 10^{-8}$ photons $\text{cm}^{-2} \text{s}^{-1}$.

References

- Abdo, A. A., et al. 2009, *Science*, 326, 1512
- Aharonian, F. A., & Atoyan, A. M. 1981, *Ap&SS*, 79, 321
- Albert, J., et al. 2007, *ApJ*, 665, L51
- Aleksić, J., et al. 2010, *ApJ*, 721, 843
- Atoyan, A. M., & Aharonian, F. A. 1999, *MNRAS*, 302, 253
- Axelsson, M., Larsson, S., & Hjalmarsdotter, L. 2009, *MNRAS*, 394, 1544
- Barbiellini, G., et al. 2002, *Nuclear Instruments and Methods in Physics Research A*, 490, 146
- Becklin, E. E., Neugebauer, G., Hawkins, F. J., Mason, K. O., Sanford, P. W., Matthews, K., & Wynn-Williams, C. G. 1973, *Nature*, 245, 302
- Bhat, C. L., Sapru, M. L., & Razdan, H. 1986, *ApJ*, 306, 587
- Bonnet-Bidaud, J. M., & Chardin, G. 1988, *Phys. Rep.*, 170, 325
- Bulgarelli, A., et al. 2012a, *A&A*, 538, A63
- Bulgarelli, A., et al. 2012b, *A&A*, 540, A79
- Cattaneo, P. W., et al. 2011, *Nuclear Instruments and Methods in Physics Research A*, 630, 251
- Cerutti, B., Dubus, G., Malzac, J., et al. 2011, *A&A*, 529, A120
- Chen, A. W., Piano, G., et al. 2011, *A&A*, 525, A33
- Coppi, P. S. 1999, *High Energy Processes in Accreting Black Holes*, 161, 375
- Corbel, S., Dubus, G., Tomsick, J. A., et al. 2012, *arXiv:1201.3356*
- Danaher, S., Fegan, D. J., Porter, N. A., & Weekes, T. C. 1981, *Nature*, 289, 568
- Dubus, G., Cerutti, B., & Henri, G. 2010, *MNRAS*, 404, L55
- Fabrika, S. N., & Borisov, N. V. 1987, *Soviet Astronomy Letters*, 13, 279
- Feroci, M., et al. 2007, *Nuclear Instruments and Methods in Physics Research A*, 581, 728
- Giacconi, R., Gorenstein, P., Gursky, H., & Waters, J. R. 1967, *ApJ*, 148, L119
- Hanson, M. M., Still, M. D., & Fender, R. P. 2000, *ApJ*, 541, 308
- Hermesen, W., et al. 1987, *A&A*, 175, 141
- H.E.S.S. Collaboration, et al. 2009, *A&A*, 508, 1135
- Hjalmarsdotter, L., Zdziarski, A. A., Szostek, A., & Hannikainen, D. C. 2009, *MNRAS*, 392, 251
- Kelner, S. R., Aharonian, F. A., & Bugayov, V. V. 2006, *Phys. Rev. D*, 74, 034018
- Koljonen, K. I. I., Hannikainen, D. C., McCollough, M. L., Pooley, G. G., & Trushkin, S. A. 2010, *MNRAS*, 406, 307
- Koljonen, K. I. I., Hannikainen, D. C., & McCollough, M. L. 2011, *MNRAS*, 416, L84
- Konigl, A. 1983, *MNRAS*, 205, 471
- Labanti, C., et al. 2006, *Proc. SPIE*, 6266
- Lamb, R. C., Godfrey, C. P., Wheaton, W. A., & Tumer, T. 1982, *Nature*, 296, 543
- Ling, Z., Zhang, S. N., & Tang, S. 2009, *ApJ*, 695, 1111
- McCollough, M. L.; et al. 1999, *ApJ*, 517, 951
- Migliari, S., Fender, R., & Méndez, M. 2002, *Science*, 297, 1673
- Mioduszewski, A. J., Rupen, M. P., Hjellming, R. M., Pooley, G. G., & Waltman, E. B. 2001, *ApJ*, 553, 766
- Mirabel, I. F. 2012, *Science*, 335, 175
- Mori, M., et al. 1997, *ApJ*, 476, 842
- O’Flaherty, K. S., et al. 1992, *ApJ*, 396, 674
- Parsignault, D. R., et al. 1972, *Nature*, 239, 123
- Perotti, F., et al. 2006, *Nuclear Instruments and Methods in Physics Research A*, 556, 228
- Piano, G., Bulgarelli, A., Tavani, M., et al. 2011, *arXiv:1110.6043*
- Pittori, C., Verrecchia, F., et al. 2009, *A&A*, 506, 1563
- Prest, M., et al. 2003, *Nuclear Instruments and Methods in Physics Research A*, 501, 280
- Reynoso, M. M., Romero, G. E., & Christiansen, H. R. 2008, *MNRAS*, 387, 1745
- Romero, G. E., Torres, D. F., Kaufman Bernadó, M. M., & Mirabel, I. F. 2003, *A&A*, 410, L1
- Romero, G. E., Christiansen, H. R., & Orellana, M. 2005, *ApJ*, 632, 1093
- Samorski, M., & Stamm, W. 1983, *ApJ*, 268, L17
- Shrader, C. R., Titarchuk, L., & Shaposhnikov, N. 2010, *ApJ*, 718, 488
- Stark, M. J., & Saia, M. 2003, *ApJ*, 587, L101
- Szostek, A., Zdziarski, A. A., 2008, *MNRAS*, 386, 593S
- Szostek, A., Zdziarski, A. A., & McCollough, M. L. 2008, *MNRAS*, 388, 1001
- Tavani, M., et al. 2009a, *Nature*, 462, 620
- Tavani, M., et al. 2009b, *A&A*, 502, 995
- Tudose, V., et al. 2007, *MNRAS*, 375, L11
- Tudose, V., et al. 2010, *MNRAS*, 401, 890
- van Kerkwijk, M. H., et al. 1992, *Nature*, 355, 703
- Vilhu, O.; et al. 2009, *A&A*, 501, 679
- Vladimirsky, B. M., Stepanian, A. A., & Fomin, V. P. 1973, *ICRC*, 1, 456
- Zdziarski, A. A., et al. 2012, *MNRAS*, 421, 2956
- Zdziarski, A. A., et al. 2012, *arXiv:1205.4402*

²⁰ The persistent AGILE-GRID source associated to Cygnus X-3 is J2033+4050 in Table 1 of [Chen, Piano et al. \(2011\)](#)

-
- ¹ INAF/IAPS, via del Fosso del Cavaliere 100, I-00133 Roma, Italy
² CIFS-Torino, viale Settimio Severo 3, I-10133 Torino, Italy
³ Dipartimento di Fisica, Università di Roma “Tor Vergata”, via della Ricerca Scientifica 1, I-00133 Roma, Italy
⁴ INAF/IASF-Milano, via E. Bassini 15, I-20133 Milano, Italy
⁵ INAF/IASF-Bologna, via Gobetti 101, 40129 Bologna, I-40129 Bologna, Italy
⁶ Dipartimento di Fisica and INFN Trieste, via Valerio 2, I-34127 Trieste, Italy
⁷ INFN-Pavia, via Bassi 6, I-27100 Pavia, Italy
⁸ INFN-Roma “Tor Vergata”, via della Ricerca Scientifica 1, I-00133 Roma, Italy
⁹ INAF-Osservatorio Astronomico di Cagliari, località Poggio dei Pini, strada 54, I-09012 Capoterra, Italy
¹⁰ ENEA Frascati, via E. Fermi 45, I-00044 Frascati (Roma), Italy
¹¹ ASI Science Data Center (ASDC), via G. Galilei, I-00044 Frascati (Roma), Italy
¹² INAF-OAR, I-00040, Via Frascati 33, Monte Porzio Catone, Italy
¹³ University of the Witwatersrand, School of Physics, WITS 2050 Johannesburg (South Africa)
¹⁴ INAF-IASF-Palermo, via U. La Malfa 15, I-90146 Palermo, Italy
¹⁵ Department of Astronomy, Yale University, P. O. Box 208101, New Haven, CT 06520-8101, USA
¹⁶ Aalto University Metsähovi Radio Observatory, Metsähovintie 114 FIN-02540 Kylmälä, Finland
¹⁷ Department of Physics and Space Sciences, Florida Institute of Technology, 150 W. University Blvd., Melbourne, FL 32901, USA
¹⁸ Smithsonian Astrophysical Observatory, 60 Garden Street, Cambridge, Massachusetts 02138, USA
¹⁹ Astrophysics Group, Cavendish Laboratory, 19 J. J. Thomson Avenue, Cambridge CB3 0HE, UK
²⁰ Special Astrophysical Observatory RAS, Karachaevo-Cherkassian Republic, Nizhnij Arkhyz 369169, Russia
²¹ Departament d’Astronomia i Meteorologia, Institut de Ciències del Cosmos, Facultat de Física, 7a planta, Universitat de Barcelona Martí i Franquès 1, 08028 Barcelona, Spain